Journal of Zhejiang University-SCIENCE A (Applied Physics & Engineering)
ISSN 1673-565X (Print); ISSN 1862-1775 (Online)
www.zju.edu.cn/jzus; www.springerlink.com
E-mail: jzus@zju.edu.cn

Ultimate stress increase in unbonded tendons in prestressed concrete beams*

Wen-zhong ZHENG, Xiao-dong WANG‡

(*Department of Civil Engineering, Harbin Institute of Technology, Harbin 150090, China*)

E-mail: zhengwenzhong@hit.edu.cn; wangxiaodong-hit@126.com

Received Oct. 16, 2009; Revision accepted July 28, 2010; Crosschecked Nov. 19, 2010

Abstract: Since the assumption of plane sections cannot be applied to the strain of unbonded tendons in prestressed concrete beams subjected to loadings, a moment-curvature nonlinear analysis method is used to develop analytical programs from stress increases in unbonded tendons at the ultimate limit state. Based on the results of model testing and simulation analysis, equations are proposed to predict the stress increase in tendons at the ultimate state in simple or continuous beams of partially prestressed concrete, considering the loading type, non-prestressed reinforcement index β_p, prestressing reinforcement index β_s, and span-depth ratio L/h as the basic parameters. Results of 380 beams studied here and test results for 35 simple beams obtained by the China Academy of Building Research were compared with those from prediction equations given in codes and other previous studies. The comparison reveals that the values predicted by the proposed equations agree well with experimental results.

Key words: Ultimate stress increase, Unbonded tendons, Loading type, Non-prestressed reinforcement index, Prestressed reinforcement index, Span-depth ratio

doi:10.1631/jzus.A0900618 **Document code:** A **CLC number:** TU3

1 Introduction

Rational evaluation of the stress increase in unbonded tendons at the ultimate state is a precondition, and the basis to exactly compute the flexural loading capacity of an unbonded prestressed concrete (UPC) beam. It is considered in the technical specification (JGJ92-2004) in China of span-depth ratio L/h and combined reinforcement index β_0. The results of 98 specimens of beams tested in (Tao, 1993) are shown in Fig. 1, from which it is seen that $\Delta\sigma_{pu}$ ($\Delta\sigma_{pu}$ is the ultimate stress increment in unbonded tendons) varies greatly even if β_0 is the same. For example, when β_0=0.3, the lowest $\Delta\sigma_{pu}$ is about 200 MPa while the highest is near 600 MPa; between the two there is a 400 MPa difference. This is due to the following reasons: first, while the combined reinforcement index β_0 is the same, non-prestressed reinforcement index β_s and prestressing reinforcement index β_p may not; second, different researchers may not choose the same indicators for the occurrence of ultimate flexural load-bearing capacity for UPC beams. To date, scholars have proposed the following different indicators to determine the ultimate load state for UPC beams:

1. The extreme concrete fiber in compressive region reaches ultimate strain.

2. Crack width reaches 1.5 mm during loading.

3. The maximum deflection reaches 1/50 of span-length.

4. The non-prestressed tensile reinforcement strain reaches 1000$\mu\varepsilon$; and/or,

5. The deformation increases while the load decreases.

In Fig.1, $\beta_0=(\sigma_{pe}A_p+f_yA_s)/(f_cbd_p)$, where σ_{pe} is the effective prestress in the prestressing steel after losses;

‡ Corresponding author

* Project supported by the National Natural Science Foundation of China (No. 50178026), the New Century Excellent Talents in University, and Changjiang Scholars Program of China (No. 2009-37)

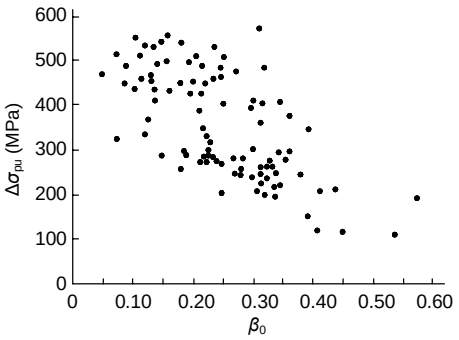

Fig. 1 $\Delta\sigma_{pu}$ versus β_0

A_p is the area of prestressing steel; f_y and A_s are yield strength and area of non-prestressed tensile reinforcement, respectively; f_c is the axial compressive strength of concrete; b is the width of the beamsection; and d_p is the depth from the extreme compression fiber of beam to the centroid of the unbonded tendons.

According to the viewpoint of this paper, the onset of ultimate load state should not be confused with a test criterion. For UPC beams, ultimate loads correspond to the ultimate state which occurs when the deformations of the beam continue to increase, whereas the loading starts to decrease. In UPC simple beams, with middle or greater level of prestress, the contribution of the stress increase in unbonded tendons to normal section loading capacity prevails over that of the decrease of the actuating arm of the internal forces during loading. Therefore, it should be taken as the sign of the ultimate state of flexural load-bearing capacity that the extreme concrete fiber in compressive region in the critical section of the UPC simple beam reaches the ultimate strain. For a UPC continuous beam, a similar sign of the ultimate state should be given; the same case appears, at least, in one span of beams where the deformations increase, but the loadings start to decrease at the ultimate load stage. Once the concrete strain in the compressive region in an intermediate support section reaches the ultimate strain ε_{cu}, part of area will not be considered as a portion of the section when the calculation is performed. As a result, the moment in the critical section at the intermediate support can be calculated; and then the moment in the critical mid-span section can be found based on static equilibrium conditions until the extreme concrete fiber in the compressive region of the critical mid-span section reaches the ultimate strain ε_{cu}.

Therefore, based on rationally selecting the failure sign for a UPC beam, it is essential to develop the equations for stress increase in unbonded tendons in the UPC beam, by considering the effect of loading types, non-prestressed reinforcement index β_s ($\beta_s=f_yA_s/(f_cbd_p)$), prestressing reinforcement index β_p ($\beta_p=\sigma_{pe}A_p/(f_cbd_p)$), span-depth ratio L/h, and numbers of span.

2 Method of analysis for partially prestressed concrete beams with unbonded tendons

2.1 Thinking of calculation

In prestressed concrete beams with unbonded tendons, the strains in the tendons are incompatible with those in the adjacent concrete, and so the assumption of plane sections fails (Tao, 1993; Ariyawardena, 2002; Barakat and Bani-Hani, 2004). According to the feature, for UPC simple beams, the constant stiffness method (A23.3-94) is applied to calculate the deformation before the non-prestressed tensile reinforcement in critical sections yields. Then the curve equations of the unbonded tendons corresponding with the deformation of the beams can be obtained, and the elongation and the strain increase of the tendons can also be computed. Subsequently, the stress increase can be calculated.

Deformation compatibility conditions for beams are introduced to solve the problem resulting from invalidation of the plane-section assumption after plastic hinges come in critical mid-span sections. It is considered that the ultimate loading capacity stage in a simple beam occurs when the concrete fiber strain in compressive region in a critical section reaches ultimate level, and a moment-curvature nonlinear method is applied to calculate the ultimate stress increase of the unbonded tendons in the UPC simple beam.

Before yielding of the non-prestressed tensile reinforcement in the critical section, the deformations and stresses in unbonded tendons can be calculated by the constant stiffness method (JGJ 92-2004) stage by stage with the application of load. The deformations due to a certain load stage may be computed, using the stress of the unbonded tendons due to the loads one stage ahead, and taking the minimum stiffness

(obtained according to the Chinese design regulation (JGJ 92-2004)) in the moment region with the same sign (positive or negative). Then the curve equation of the unbonded tendons corresponding with the deformation curve of the beam can be obtained, and the elongation and the strain increase of the tendons can be computed by integrating the curve equation of the tendons. Finally, the unbonded tendons stress under the loads considered can be calculated based on the stress-strain curve of the unbonded tendons.

After the non-prestressed tensile reinforcement in the critical intermediate support section yields, the internal force of the structure under the new added load may be calculated by the method of simple beams. Considering the contribution of the stress increase in the unbonded tendons (the stress increase during the process from the time when the non-prestressed tensile reinforcement in the critical mid-span section starts yielding to that when the non-prestressed tensile reinforcement in the critical intermediate support section yields) to the flexural load-bearing capacity in the critical intermediate support section, the deformation under the loading can still be calculated according to the principle of constant stiffness in each moment region with the same sign. With the load increasing, after the non-prestressed tensile reinforcement in the critical intermediate support section yields, the contribution of the stress increase $\Delta\sigma_p$ (relative to the state when the non-prestressed tensile reinforcement in the critical intermediate support section yields) to flexural load-bearing capacity in the critical intermediate support section can be approximately calculated as $\Delta M=0.85d_p\Delta\sigma_pA_p$. This iterative calculation process will not be completed until the non-prestressed tensile reinforcement in the critical mid-span section yields (Ariyawardena, 2002).

After the non-prestressed tensile reinforcement in the critical mid-span section yields, i.e., as long as a plastic hinge occurs in that section, deformation compatibility in the whole beam is considered to solve the problem of the non-valid assumption of plane-section, and therefore a non-linear moment-curvature method is adopted. Because the load does not reach the ultimate even if the extreme concrete fiber in compressive region reaches ultimate stain ε_{cu} in critical intermediate support sections in a continuous beam, it should be considered that the ultimate load stage is reached. Thus, it is considered that the structure has reached its ultimate load-bearing stage when the deformation continues to increase, whereas the load starts to decrease.

The method applied in this study is obtained as follows: After the non-prestressed tensile reinforcement in the critical mid-span section of the beam yields and a plastic hinge occurs there, the deformation cannot be calculated by the constant stiffness method. For this reason, the beam to be calculated is partitioned into segments from zero moment section (the section of outer supports and points of contra-flexure) to crack moment section; from crack moment section to the yielding moment section; and from yielding moment section to the ultimate moment section. Each of the segments is further sub-divided into a number of smaller segments. Then the strain of concrete at the level of prestressing steel in every small segment is calculated, and all the strains of the tiny segments in every region along the beams are summed up to determine the total stress increase of the unbonded tendon based on the relationship of stress and strain for the tendon (Du and Tao, 1985; Harajli, 1990; Chen and Zhao, 1993; BS8110-1-1997; Barakat and Bani-Hani, 2004; Zhou, 2005). This is a dynamic process because points of contra-flexure change with time during the loading.

Note that because the stress increases very little in unbonded tendons, it is stipulated in Chinese design specification (JGJ 92-2004) that when effective prestress in tendons is calculated, the influence of tensile σ_{pc} (σ_{pc} is normal stress in concrete due to prestressing force) on shrinkage creep loss and that of flexural deformation in beams on effective prestress are not taken into account. Therefore, the initial time is set when the stretching of unbonded tendons is completed and the initial prestresses become the effective prestresses in accordance with design specification.

2.2 Method of analysis for ultimate stress in unbonded tendons

2.2.1 UPC simple beams

Consider, for example, that a simple prestressed concrete beam with straight unbonded tendons under third point loads (can also be applied for the uniform loads). The constant stiffness method is non-valid after the non-prestressed tensile reinforcement yields

and a plastic hinge occurs in the critical mid-span section of the beam. For this reason, first assume the stress of unbonded tendons equals to the effective stress σ_{pe}, then the moment diagram is divided into a number of regions, and correspondingly the beam into the same number of segments to calculate the stress of unbonded tendons: region IV is the ultimate moment distribution region; region III from the ultimate moment section to the yielding moment section; region II from the yielding moment section to the crack moment section; region I from the crack moment section to the support section. Each of them is sub-divided into a number of very small regions. Then the strain of concrete at the level of the prestressing steel in every segment is calculated. Finally, a summation is made for all the strains above each region to determine the total stress increase of the unbonded tendons based on the relationship of stress and strain of the tendons. Then compare the calculated stress of unbonded tendons to the assumed one. If they are not within the specified tolerance, repeat the process again mentioned above, but take the calculated unbonded tendons stress as the new assumed unbonded tendons stress. This will not stop until the calculated stress and the assumed stress match well. Then the stress calculated will be the real ultimate stress of unbonded tendons.

As shown in Fig. 2, take a simple prestressed concrete beam under third point loads for example (which can also be applied for the uniform loads). After non-prestressed tensile reinforcement in a critical mid-span section yields, we assume the stress of unbonded tendons equals to the effective stress σ_{pe}. There are four critical sections in the beam: a constant moment section in mid-span; the section where non-prestressed tensile reinforcement just reaches to yielding stress; concrete crack section; and border support section. The strain of the extreme concrete fiber in the tensile region of the cracked section is given by $\varepsilon=\gamma f_{tk}/E_c$ (where γ is the plastic influence coefficient of section modulus of the concrete member; f_{tk} axial compressive strength of the concrete; E_c modulus of elasticity of the concrete). The strain of steel in non-prestressed tensile yielding section is $\varepsilon_y=f_y/E_s$. The ultimate strain of the extreme fiber of concrete in compressive region $\varepsilon_{cu}=0.0033$. Assuming the stress of tendon, an iterative method for M-ϕ (where M is moment and ϕ is curvature) is adopted to calculate the section crack moment M_{cr}, the yielding moment M_y, the ultimate moment M_u and the corresponding crack curvature ϕ_{cr}, the yielding curvature ϕ_y, the ultimate curvature ϕ_u and the neutral axis depth in the crack section C_{cr}, the neutral axis depth in the yield section C_y, and the neutral axis depth in the ultimate section C_u (Tao *et al*., 1989).

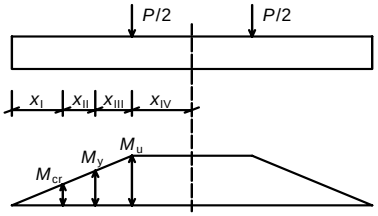

Fig. 2 Moment diagram of the simple beam subjected to ultimate load

M_{cr} is the section crack moment, M_y is the yielding moment, M_u is the the ultimate moment, x_I, x_{II}, x_{III} and x_{IV} are the lengths of segments, and P is the load

From the above analysis, and considering symmetry, the beam can be divided into 8 segments (or regions) as shown in Fig. 2. The moment, the curvature and the neutral axis depth are assumed to have linear distribution in every segment. After the length of every segment, x_I, x_{II}, x_{III} and x_{IV}, calculated and every segment divided into quite a number of tiny regions, then the segment elongations ΔI_1, ΔII_1, ΔIII_1 and ΔIV_1 at the level of the prestressing steel along the beam can be calculated based on the moment-curvature relationship and the method of the plane-section assumption:

$$\begin{cases} \Delta \mathrm{IV}_1 = \sum \phi_{ui}(d_p - c_{ui})\Delta x_{IV}, \\ \Delta \mathrm{III}_1 = \sum \phi_{yi}(d_p - c_{yi})\Delta x_{III}, \\ \Delta \mathrm{II}_1 = \sum \phi_{cri}(d_p - c_{cri})\Delta x_{II}, \\ \Delta \mathrm{I}_1 = \sum \phi_{endi}(d_p - c_{endi})\Delta x_I, \end{cases} \quad (1)$$

where ϕ_{ui}, c_{ui} are the curvature and the neutral axis depth, respectively, in the ith segment in the constant moment segment x_{IV}; ϕ_{yi}, c_{yi} the curvature and neutral axis depth, respectively, in the ith segment in the non-prestressed steel yielding segment x_{III}; ϕ_{cri}, c_{cri} the curvature and the neutral axis depth, respectively, in the ith segment in the concrete crack appearance segment x_{II}; ϕ_{endi}, c_{endi} the curvature and the neutral axis depth, respectively, in the ith segment in the border support segment x_I.

The total concrete elongation at the level of the prestressing steel along the beam can be calculated as follows:

$$\Delta l_p=2(\Delta I_1+\Delta II_1+\Delta III_1+\Delta IV_1). \quad (2)$$

The stress increase in the unbonded tendons is

$$\Delta\varepsilon_p=\Delta l_p/l_{po}, \quad (3)$$

where l_{po} is the total length of tendon after tensioning and before the beam is loaded.

The strain in unbonded tendon is

$$\varepsilon_p=\varepsilon_{pe}+\Delta\varepsilon_p, \quad (4)$$

where ε_{pe} is the strain in the tendon corresponding to the effective prestress σ_{pe}.

Based on the stress-strain relationship of the prestressing steel, the ultimate stress σ_p in the unbonded tendons can be calculated. The stress increase $\Delta\sigma_{pu}$ in the unbonded tendons at the ultimate state can be expressed as

$$\Delta\sigma_{pu}=\sigma_p-\sigma_{pe}. \quad (5)$$

Then compare the calculated stress of unbonded tendons to the assumed one. If the calculated stress and the assumed stress do not match, repeat the process again. Then the stress calculated will be the real ultimate stress of unbonded tendons.

2.2.2 UPC continuous beams

Continuous beams can be analysed by adopting the method used for simple beams. We study a part of one span continuous beam, for example, from the border support to the center of the plastic hinge region in the mid-span. Assume the stress of unbonded tendons equals to the effective stress σ_{pe}, and then this part of beam is divided into three segments as shown in Fig. 3: I, II and III. Assuming the distribution of the moment, the curvature and the neutral axis depth are linear in every segment, respectively; then the length of every segment, x_I, x_{II} and x_{III} can be calculated based on the moment equilibrium equation. Dividing each segment into quite a number of very small segments, the elongation ΔI_2, ΔII_2 and ΔIII_2 at the level of the prestressing steel along the beam can be calculated, respectively, based on the moment-curvature relationship and the method of the plane-section assumption:

$$\begin{cases}\Delta III_2=\sum\phi_{yi}(d_{pi}-c_{yi})\Delta x_{III},\\ \Delta II_2=\sum\phi_{cri}(d_{pi}-c_{cri})\Delta x_{II},\\ \Delta I_2=\sum\phi_{endi}(d_{pi}-c_{endi})\Delta x_{I},\end{cases} \quad (6)$$

where ϕ_{yi}, c_{yi} are the curvature and neutral axis depth, respectively, in the ith segment in segment III; ϕ_{cri}, c_{cri} the curvature and neutral axis depth, respectively, in the ith segment in segment II; ϕ_{endi}, c_{endi} the curvature and neutral axis depth, respectively, in the ith segment in segment I.

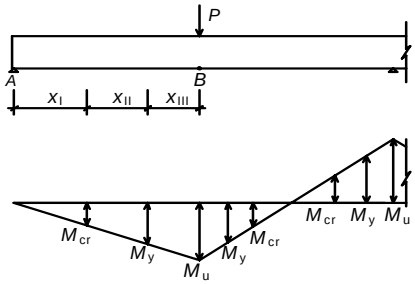

Fig. 3 Moment diagram of the continuous beam subjected to ultimate load

M_{cr} is the section crack moment, M_y is the yielding moment, M_u is the ultimate moment, x_I, x_{II}, x_{III} and x_{IV} are the lengths of segments, and P is the load

The concrete elongation at the level of the prestressing steel in the part of the beam studied, *AB*, can be calculated as follows:

$$\Delta l_p=\Delta I_2+\Delta II_2+\Delta III_2. \quad (7)$$

The concrete elongation at the level of the prestressing steel in the other parts of the beam can be calculated by similar methods, then stress and the stress increase in the unbonded tendons at the ultimate state can be found. Then compare the calculated stress of unbonded tendons to the assumed one. If they are not within the specified tolerance, repeat the process again mentioned above, but take the calculated unbonded tendons stress as the new assumed unbonded tendons stress, and this will not stop until the calculated stress and the assumed stress match well. Then the stress calculated will be the real ultimate stress of unbonded tendons.

2.2.3 Verification of the analysis

In the experimental study on 18 specimens of a partially UPC simple beam conducted by Tao *et al.* (1989) in the China Academy of Building Research, the specimens with cross-section $b\times h$=160 mm×280 mm or 400 mm×160 mm in two groups were tested under a concentrated load at mid-span or under two symmetrical third-point loads. Other details of test beams are shown in Table 1. $\bar{x}$ is the mean value and σ is the standard deviation of the ratio ($x=\sigma_{pu}^{c}/\sigma_{pu}^{t}$).

In the experimental study on 16 specimens of a partially UPC simple beam obtained by Du and Tao (1985) in the China Academy of Building Research, all of the specimens with the same cross-section $b\times h$=160 mm×280 mm were tested under two third point loads. Other details of test beams are shown in Table 2.

Table 1 Comparison between the data in (Tao *et al.*, 1989) and calculated results ($\bar{x}$ =1.015, σ=0.034)

Beam No.	f_{cu} (MPa)	l (mm)	A_p (mm^2)	A_s (mm^2)	σ_{pe} (MPa)	σ_p (MPa)		$x=\sigma_{pu}^{c}/\sigma_{pu}^{t}$
						σ_{pu}^{t}	σ_{pu}^{c}	
10M1	56.0	2400	58.8	157	951	1504	1539	1.024
10M2	60.0	2400	98.0	236	950	1447	1444	0.998
10M3	60.0	2400	137.2	509	933	1232	1322	1.073
10T1	52.0	2400	58.8	157	1019	1551	1550	0.999
10T2	52.0	2400	98.0	236	933	1471	1473	1.001
10T3	52.0	2400	137.2	509	928	1222	1356	1.110
20M1	56.0	4600	58.8	157	915	1437	1446	1.006
20M2	56.0	4600	98.0	236	895	1328	1367	1.030
20M3	56.0	4600	137.2	509	958	1196	1247	1.043
20T1	52.0	4600	58.8	157	951	1517	1548	1.020
20T2	53.1	4600	98.0	236	982	1485	1491	1.004
20T3	56.0	4600	137.2	509	911	–	–	–
40M1	60.0	5000	78.4	157	955	1435	1404	0.978
40M2	60.0	5000	156.8	314	879	1247	1199	0.962
40M3	60.0	5000	274.0	481	900	1090	1077	0.988
40T1	53.1	5000	78.4	157	931	1542	1563	1.013
40T2	54.0	5000	156.8	314	937	1411	1418	1.005
40T3	54.0	5000	274.4	481	916	1251	1242	0.993

f_{cu}: compressive cube strength; σ_{pu}^{c}: ultimate stress in the unbonded tendons predicted by the proposed method; σ_{pu}^{t}: ultimate stress of test results

Table 2 Comparison between the data in (Tu and Tao, 1985) and calculated results ($\bar{x}$ =1.020, σ=0.035)

Beam No.	f_{cu} (MPa)	l (mm)	A_p (mm^2)	A_s (mm^2)	σ_{pe} (MPa)	σ_p (MPa)		$x=\sigma_{pu}^{c}/\sigma_{pu}^{t}$
						σ_{pu}^{t}	σ_{pu}^{c}	
A-1	36.0	4200	58.8	157	960	1458	1469	1.007
A-2	36.0	4200	98.0	157	904	1430	1375	0.962
A-3	36.0	4200	156.8	236	820	1176	1218	1.035
A-4	36.0	4200	58.8	157	869	1465	1435	0.979
A-5	36.0	4200	78.4	308	810	1315	1325	1.008
A-6	36.0	4200	156.8	462	854	1063	1144	1.076
A-7	36.0	4200	39.2	308	885	1436	1389	0.967
A-8	38.9	4200	58.8	462	894	1290	1336	1.035
A-9	38.9	4200	156.8	804	920	1108	1120	1.011
B-1	53.9	4200	58.8	157	1008	1645	1655	1.006
B-2	53.9	4200	98.0	157	987	1564	1577	1.008
B-3	50.0	4200	156.8	236	963	1361	1463	1.075
B-5	50.0	4200	78.4	308	989	1520	1534	1.009
B-6	50.0	4200	137.2	462	1002	1402	1432	1.021
B-7	57.4	4200	39.2	308	1002	1603	1684	1.050
B-9	57.4	4200	98.0	804	1050	1346	1451	1.078

f_{cu}: compressive cube strength; σ_{pu}^{c}: ultimate stress in the unbonded tendons predicted by the proposed method; σ_{pu}^{t}: ultimate stress of test results

In the experimental study on 2 specimens of a partially UPC simple beam by Liu and Chen (2003), the two specimens with the same cross-section $b \times h$=150 mm×300 mm were tested under two third point loads. Other details of test beams are shown in Table 3.

In the experimental study on 16 specimens of a partially UPC continuous beam conducted by Wang (2005), all the specimens with the same cross-section $b \times h$=200 mm×300 mm were tested under a concentrated mid-span load. Other details of test beams are shown in Table 4.

Statistical analysis indicates that the ultimate stress (σ_{pu}^{c}) in the unbonded tendons predicted by the proposed method are similar to the test results (σ_{pu}^{t}) from the tests mentioned above, and the mean value $\overline{x}$ and the standard deviation σ of the ratio of ($\sigma_{pu}^{c} / \sigma_{pu}^{t}$) are shown in Tables 1–4, respectively. The results show that the stress increases in the tendons predicted by the proposed method agree well with the test results, and the calculation program for the ultimate stress in tendons in UPC beams developed in this study have sufficient precision to be used for analysis.

2.3 Experimental results and analysis

2.3.1 Simulated beams

For continuous beams, secondary moment will be caused by stretching the tendons, and the moment in the intermediate critical support sections. So the simulated beam specimens in this study were reinforced with same amounts of prestressing steel and non-prestressed steel in intermediate support and mid-span sections. The simulated simple and continuous beam specimens can be grouped based on different parameters considered as follows:

Table 3 Comparison between the data in (Liu and Chen, 2003) and calculated results ($\overline{x}$ =0.978, σ=0.017)

Beam No.	f_{cu} (MPa)	l (mm)	A_p (mm^2)	A_s (mm^2)	σ_{pe} (MPa)	σ_p (MPa)		$x=\sigma_{pu}^{c}/\sigma_{pu}^{t}$
						σ_{pu}^{t}	σ_{pu}^{c}	
A-1	33.4	2500	140	226	960	1234	1240	1.005
B-1	33.4	2500	140	509	904	1081	1125	1.041

f_{cu}: compressive cube strength; σ_{pu}^{c}: ultimate stress in the unbonded tendons predicted by the proposed method; σ_{pu}^{t}: ultimate stress of test results

Table 4 Comparison between the data in (Wang, 2005) and calculated results ($\overline{x}$ =1.045, σ=0.112)

Beam No.	f_{cu} (MPa)	l (mm)	A_p (mm^2)	A_{s1} (mm^2)	A_{s2} (MPa)	σ_{pe} (MPa)	σ_p (MPa)		$x=\sigma_{pu}^{c}/\sigma_{pu}^{t}$
							σ_{pu}^{t}	σ_{pu}^{c}	
YLA-4	32.1	3000	78.5	211	710	1088	1624	1455	0.896
YLC-2	32.0	3000	333.7	293	710	853	1336	1175	0.880
YLD-3	29.5	3000	353.3	519	534	989	1161	1251	1.078
YLB-1	33.6	3000	176.7	437	936	730	1059	1144	1.080
YLB-3	32.0	3500	215.9	211	760	1004	1139	1312	1.152
YLC-4	32.1	3500	176.7	695	986	1124	1286	1326	1.031
YLA-2	29.5	3500	117.8	169	760	862	1014	1321	1.302
YLD-1	33.6	3500	392.6	695	710	743	940	1001	1.065
YLA-1	32.0	4000	137.4	169	710	749	1065	1293	1.214
YLB-4	33.6	4000	176.7	293	760	1136	1316	1352	1.028
YLC-3	29.5	4000	235.6	519	911	1012	1364	1286	0.943
YLD-2	32.1	4000	274.8	839	854	874	1082	1141	1.055
YLA-3	33.6	4500	58.9	211	628	1017	1485	1432	0.964
YLD-4	29.5	4500	373.0	387	402	1146	1460	1311	0.898
YLC-1	32.0	4500	333.7	387	760	756	1005	1041	1.036
YLB-2	32.1	4500	176.7	387	804	880	1165	1285	1.103

f_{cu}: compressive cube strength; σ_{pu}^{c}: ultimate stress in the unbonded tendons predicted by the proposed method; σ_{pu}^{t}: ultimate stress of test results

1. Loading type: beams under a single mid-span load, third point load, or uniformly distributed load, respectively.

2. Prestressing reinforcement index β_p in the critical sections: beams with β_p=0.05, 0.10, 0.15, 0.20, respectively.

3. Non-prestressing reinforcement index β_s in the critical sections: beams with β_s=0.05, 0.07, 0.09, 0.11, 0.13, 0.15, 0.17, 0.19, 0.21, 0.23, respectively.

4. Span-depth ratio L/h: beams with L/h=10, 20, 30, 40, respectively.

2.3.2 Prediction equations for ultimate stress in unbonded tendons

1. Prediction equations for the stress increase in the unbonded tendons in simple concrete beams at an ultimate state

The stress increase $\Delta\sigma_{pu}$ in the unbonded tendons in a simple concrete beam at an ultimate state can be considered as a function of loading types, non-prestressed reinforcement index β_s, and prestressing reinforcement index β_p. Based on the results of the simulation analysis, the envelopes of $\Delta\sigma_{pu}$ versus β_s and β_p are drawn in Fig. 4 for the simulated simple beam under different types of loadings. The span-depth ratio of the beam is 20.

Calculation analysis indicates that span-depth ratio L/h has little effect on the ultimate stress increase of the unbonded tendons in the simple beam under two third point loads or uniform loads.

The ultimate stress increase in the unbonded tendons for a simple beam under various cases of loads may be predicted as follows:

Case 1, two third point loads:

$$\Delta\sigma_{pu}=663-1131\beta_p-703\beta_s. \quad (8)$$

Case 2, uniform loads:

$$\Delta\sigma_{pu}=631-1144\beta_p-753\beta_s. \quad (9)$$

Case 3, a mid-span single load:

$$\Delta\sigma_{pu}=(560-1449\beta_p-837\beta_s)(0.86+2.4h/L). \quad (10)$$

Let δ be the variation coefficient of the ratio $\Delta\sigma_{pu}^{c}/\Delta\sigma_{pu}^{t}$. Statistical analysis indicates that $\overline{x}=0.99$, σ=0.025 and δ=0.025 when $\Delta\sigma^{c}$ is predicted by Eqs. (8) and (9), and $\overline{x}=0.99$, σ=0.121 and δ=0.134 when $\Delta\sigma^{c}$ is predicted by Eq. (10). It is proved that the stress increase in the tendons predicted by Eqs. (8)–(10) agrees with the test results well, and the prediction equations (Eqs. (8)–(10)) have adequate precision.

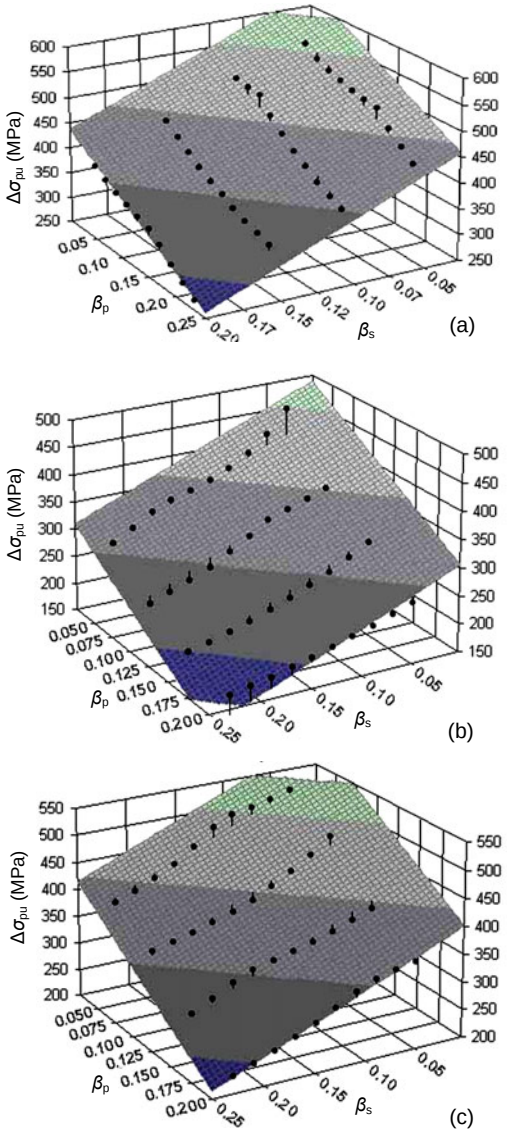

Fig. 4 Fitting surfaces of $\Delta\sigma_{pu}$ versus β_s and β_p for simple concrete beams

(a) A mid-span single loading; (b) two third point loading; (c) uniform loadings

Moreover, the simulation analysis indicates that there exists little influence of the form of tendon profile (straight or parabolic) on the ultimate stress increase in unbonded tendons. Note that Eqs. (8)–(10) apply to simple beams with combined reinforcement index $\beta_0=\beta_s+\beta_p\leq 0.4$.

2. Prediction equations for the stress increase in unbonded tendons in continuous concrete beams at an ultimate state

Based on the results of simulation analysis, the envelopes of $\Delta\sigma_{pu}$ versus β_s and β_p are drawn in Fig. 5 for a simulated two-span continuous concrete beam under different types of loading. The span-depth ratio of the beam is 20.

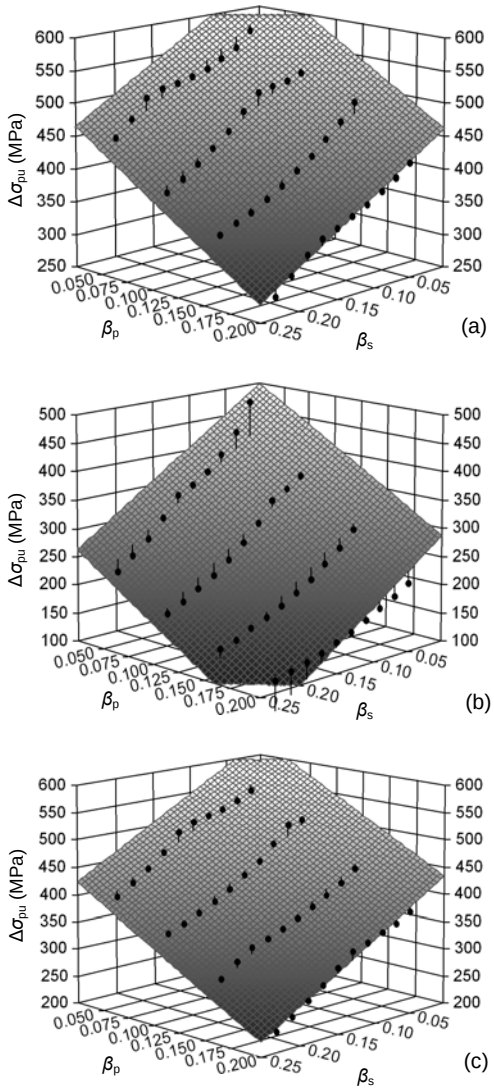

Fig. 5 Fitting surfaces of $\Delta\sigma_{pu}$ versus β_s and β_p in two-span concrete continuous beams
(a) A mid-span single loading; (b) two third point loading; (c) uniform loadings

Due to complication of the influence of factors on the ultimate stress in the unbonded tendons in continuous beams, the stress increase in the unbonded tendons at an ultimate state is regarded as the function of non-prestressing reinforcement index β_s, prestressing reinforcement index β_p and span-depth ratio L/h, and is predicted for the continuous beams with span-depth ratio 10, 20, 30, 40 in each group. For beams with other span-depth ratios, the stress increase in the unbonded tendons can be calculated by the interpolation method.

Calculation analysis indicates that there is little effect of span-depth ratio on the ultimate stress increase in unbonded tendons in continuous beams under third point or uniform loads.

The ultimate stress increases in unbonded tendons in continuous beams under various loading cases are predicted as follows:

Case 1: two third point loads:

$$\Delta\sigma_{pu}=677-1075\beta_p-741\beta_s. \quad (11)$$

Case 2: uniform loads:

$$\Delta\sigma_{pu}=659-1128\beta_p-833\beta_s. \quad (12)$$

Case 3: a single mid-span load:

The ratio of span to depth has a large influence on the stress increase in unbonded tendons in continuous beams in this case, and the corresponding prediction equation is given as follows:

$$\Delta\sigma_{pu}=\begin{cases}632-1408\beta_p-834\beta_s, & L/h=10,\\ 584-1287\beta_p-918\beta_s, & L/h=20,\\ 575-1266\beta_p-941\beta_s, & L/h=30,\\ 580-1290\beta_p-953\beta_s, & L/h=40.\end{cases} \quad (13)$$

Eq. (13) can be simplified into a single prediction equation:

$$\Delta\sigma_{pu}=(632-1408\beta_p-834\beta_s)[0.8+2/(L/h)]. \quad (14)$$

Statistical analysis indicates that $\overline{x}=1.00$, σ=0.025 and δ=0.025 when $\Delta\sigma^c$ is predicted by Eqs. (11), (12), or (14) as compared with the test results for $\Delta\sigma_{pu}$. It is proved that the stress increase in tendons predicted by Eqs. (11), (12), or (14) agrees with the test results. Note that Eqs. (11), (12) or (14) apply to the continuous beams with combined reinforcement index β_0<0.4 (Zheng *et al.*, 2005).

2.3.3 Formulas for ultimate stress in unbonded tendons in concrete beams

The ultimate stress in unbonded tendons in concrete beams is given as

$$\sigma_{pu}=\sigma_{pe}+\Delta\sigma_p, \tag{15}$$

and the design value of which can be temporarily calculated as follows:

$$\sigma_{pu}=(\sigma_{pe}+\Delta\sigma_{pu}/n)/1.2. \tag{16}$$

The design value σ_{pu} also needs to satisfy the following requirements:

$$\sigma_{pe}\leq\sigma_{pu}\leq f_{py}, \tag{17}$$

where n is the number of continuous beam spans with approximately equal length, and f_{py} is the yielding stress of the prestressing steel.

Note that n=1 for simple beams. It is impossible in engineering that all spans are overloaded and reach their ultimate carrying capacity state simultaneously for continuous beams, thus, $\Delta\sigma_{pu}$ is divided by n in Eq. (16) temporarily. Certainly, there is the need to conduct a study of the stress increase in unbonded tendons in multi-span ($n\geq3$) continuous beams.

2.4 Comparison and analysis of existing prediction equations

To justify the rationality of the prediction equations for the stress increase in unbonded tendons at ultimate state proposed in this study, and to have a macroscopical apprehension to the precision of ones recommended in relative codes and references, the results from the analysis of 380 simulated beams and tests of 35 simple beams conducted at the China Academy of Building Research are compared with ones from the prediction equations given in codes, such as ACI318-02, BS8110-1-1997, A23.4-94, DIN4227 and NZS3101 (Wang, 2005), JGJ/T92-93 (Zhou, 2005), JGJ 92-2004 (Zheng *et al.*, 2005) and by studies of Jin *et al.* (2000), Harajli Eq. (I) and Eq. (II) (Harajli, 1990), Du and Tao (1985), Xu *et al.* (1995), Chen and Zhao (1993), and Naaman and Alkhairi (1991). $\Delta\sigma_{pu}^{c}$ (predicted) versus $\Delta\sigma_{pu}^{t}$ (experimental) are drawn for all the equations in Figs. 6–20, and the discrepancies between $\Delta\sigma_{pu}^{c}$ and $\Delta\sigma_{pu}^{t}$ are examined intuitively according to the plots, how well they approach the correlation line of inclination 45° is also obtained.

The objects of simulation analysis are simple or continuous beams subjected to a mid-span point load or two third point loads or uniform loading in every span. The equation predicting the ultimate stress in unbonded tendons in current Chinese technical specification (JGJ 92-2004) for prestressed concrete structures with unbonded tendons applies to $\beta_0\leq0.40$. For the ratio of compressive strength of concrete between tested and design values is greater than that of the tested tensile yielding strength to the design tension strength for steel, one sets the combined reinforcement index $\beta_0^{t}\leq0.35$ in simulated beams.

The followings are the comparison analyses of stress increase $\Delta\sigma_{pu}^{c}$ in unbonded tendons predicted by equations with testing results $\Delta\sigma_{pu}^{t}$. Note that in the following figures the solid plots correspond to simple beams, and hollow ones to continuous beams.

1. Equation from ACI318-02

$$\sigma_{pu}=\begin{cases}\sigma_{pe}+70+\dfrac{f_c'}{100\rho_p}, & L/d_p\leq35, \quad (a)\\ \sigma_{pe}+70+\dfrac{f_c'}{300\rho_p}, & L/d_p>35, \quad (b)\end{cases} \tag{18}$$
$$\sigma_{pu}\leq f_{py},\ \sigma_{pe}\geq0.5f_{ptu},$$

where f_c' is the compressive cylinder concrete strength, $f_c'=0.8f_{cu}$, f_{cu} is the compressive cube strength, f_{ptu} is the tensile strength of the unbonded tendons, and ρ_p is the pre-stressing steel ratio, $\rho_p=A_p/(bh_p)$.

Note that Eq. (18a) is valid for $\sigma_{pu}\leq\sigma_{pe}+414$ and Eq. (18b) for $\sigma_{pu}\leq\sigma_{pe}+207$; both equations should not exceed the conditional yielding strength of the pre-stressed steel, and $\sigma_{pe}\geq0.5f_{ptk}$.

Adopting the average value of the tested strength of the material in the tested beams to Eq. (18) results in $\Delta\sigma_{pu}^{c}$. The comparison of $\Delta\sigma_{pu}^{c}$ with $\Delta\sigma_{pu}^{t}$ is shown in Fig. 6. In Fig. 6, very few data points are

over the correlation line of inclination 45°; thus, Eq. (18) predicts conservative values, and the deviation increases with increasing $\Delta\sigma_{pu}^{t}$. This is due to the equation not taking the effect of non-prestressed tensile steel and the type of loads into account; thus, the prediction values for beams under two third point loads or uniform loads are much lower than the test results.

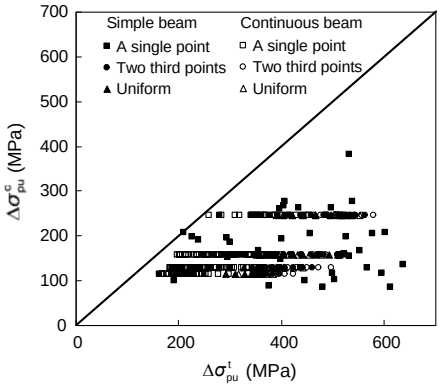

Fig. 6 Comparison between $\Delta\sigma_{pu}^{t}$ and $\Delta\sigma_{pu}^{c}$ from Eq. (18)

2. Equation from BS8110-1-1997

$$\sigma_{pu}=\sigma_{pe}+\frac{7000}{L/d_{p}}\left(1-\frac{1.7f_{ptu}A_{p}}{f_{cu}bd_{p}}\right)\le 0.7f_{ptu}. \quad (19)$$

Substituting the average test values of the material strength of the test beams into Eq. (19) leads to $\Delta\sigma_{pu}^{c}$. The comparison of $\Delta\sigma_{pu}^{c}$ with $\Delta\sigma_{pu}^{t}$ is shown in Fig. 7, where few data points are over the correlation line; thus, Eq. (19) predicts conservative values, and the deviation increases with increasing $\Delta\sigma_{pu}^{t}$. This is due to the fact that Eq. (19) considers only the effect of span-depth ratio and prestressing reinforcement index, but ignores the effect of non-prestressed tensile steel and the type of loading. If the beams were reinforced with the same amount of prestressing steel but different non-prestressing steel, the ultimate deformation would be different. For the same testing beam but under different loads, because the deformation will be different, the stress increase at ultimate will be different, too. For a few of data plots, $\Delta\sigma_{pu}^{c}$ are larger than $\Delta\sigma_{pu}^{t}$ because they correspond to the beams under a single point load and the deformation is relatively small.

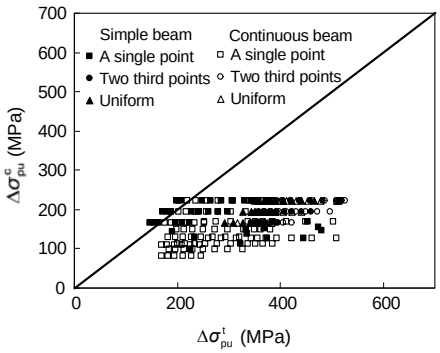

Fig. 7 Comparison between $\Delta\sigma_{pu}^{t}$ and $\Delta\sigma_{pu}^{c}$ from Eq. (19)

3. Equation from A23.3-94

$$\sigma_{pu}=\sigma_{pe}+8000\frac{(d_{p}-C_{y})}{L_{e}}\le f_{py}, \quad (20)$$

where f_{py} is the tensile strength of the prestressed steel; C_y the depth from the extreme compressive concrete fiber to the neutral axis calculated using f_{py}; L_e the span length between end anchorages divided by the number of plastic hinges.

Adopting the material strength of test beams to Eq. (20), $\Delta\sigma_{pu}^{c}$ is predicted. The comparison of $\Delta\sigma_{pu}^{c}$ with $\Delta\sigma_{pu}^{t}$ is shown in Fig. 8, where most data plots are under the correlation line, so Eq. (20) predicts conservative values. This is because the equation takes into account only the effect of span-depth ratio and prestressing reinforcement index, but ignores the effect of non-prestressed tensile steel and the type of loading, which results in Eq. (20) predicting lower values for the beams under two third point or uniform loads, but slightly higher values for ones under a mid-span point load.

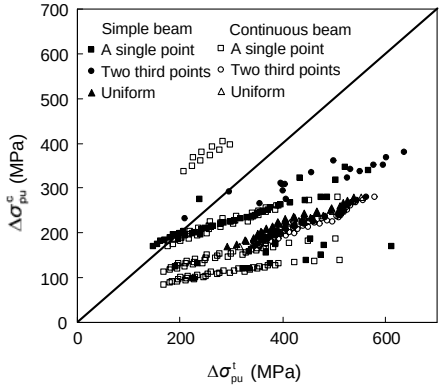

Fig. 8 Comparison between $\Delta\sigma_{pu}^{t}$ and $\Delta\sigma_{pu}^{c}$ from Eq. (20)

4. Equation from DIN4227 (Harajli, 1990)

Single span beams: $\sigma_{pu}=\sigma_{pe}+110$, (21a)
cantilever beams: $\sigma_{pu}=\sigma_{pe}+50$, (21b)
continuous beams: $\sigma_{pu}=\sigma_{pe}$. (21c)

The comparison between $\Delta\sigma_{pu}^{t}$ and $\Delta\sigma_{pu}^{c}$ from Eq. (21) is shown in Fig. 9, where all the data plots are under the correlation line; thus, Eq. (21) predicts conservative values.

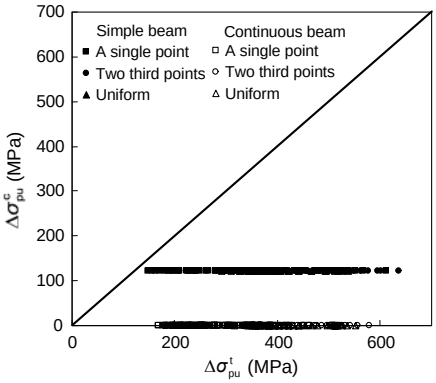

Fig. 9 Comparison between $\Delta\sigma_{pu}^{t}$ and $\Delta\sigma_{pu}^{c}$ from Eq. (21)

5. Equation from NZS3101 (Harajli, 1990)

$$\sigma_{pu}=\sigma_{pe}+100. \tag{22}$$

The comparison of $\Delta\sigma_{pu}^{c}$ predicted by Eq. (22) with the test results $\Delta\sigma_{pu}^{t}$ is shown in Fig. 10. Similar to the German code DIN4227, the New Zealand code predicts NZS3101 conservative values.

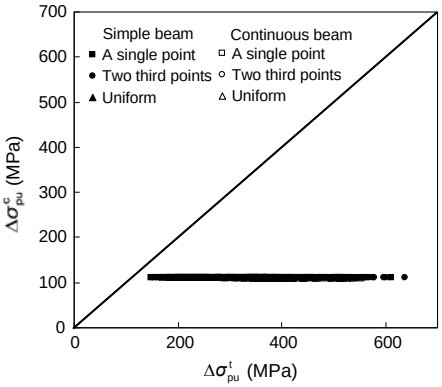

Fig. 10 Comparison between $\Delta\sigma_{pu}^{t}$ and $\Delta\sigma_{pu}^{c}$ from Eq. (22)

6. Chinese regulations JGJ/T92-93 for unbonded prestressed concrete technology

$$\sigma_{pu}=\begin{cases}\dfrac{\sigma_{pe}+(500-770\bar{\beta}_0)}{1.2}, & L/d_p\le 35,\\ \dfrac{\sigma_{pe}+(250-380\bar{\beta}_0)}{1.2}, & L/d_p>35,\end{cases} \tag{23}$$

$$\sigma_{pe}\le\sigma_{pu}\le f_{py},$$

$$\bar{\beta}_0\le 0.45,\ \ \bar{\beta}_0=(A_p\sigma_{pe}+A_s f_y)/(f_{cm}bd_p).$$

This yields the predicted $\Delta\sigma_{pu}^{c}$ to multiply the design value of the ultimate stress in the tendons predicted by Eq. (23) by subentry coefficient γ_s of the material strength of the prestressed reinforcement (γ_s=1.2 in Chinese unbonded prestressed concrete structure specification), and to subtract the effective prestress σ_{pe} in the unbonded tendons. When calculating $\bar{\beta}_0$, f_y is the tested value of yielding stress of the non-prestressing steel and f_{cm} one of conceret compressive strength. In Fig. 11, most plots of $\Delta\sigma_{pu}^{c}$ have lower values than $\Delta\sigma_{pu}^{t}$ and as a whole, the data of $\Delta\sigma_{pu}^{c}$ and $\Delta\sigma_{pu}^{t}$ are greatly scattered. This is mainly due to the beams under two third point or uniform loads suffering comparatively large ultimate deformation and $\Delta\sigma_{pu}^{t}$ with high values, and due to the beams under a mid-span point load suffering comparatively small ultimate deformation and $\Delta\sigma_{pu}^{t}$ with small values. Furthermore, Eq. (23) does not take into account the effect of the distribution of prestressing reinforcements, number of spans and the same $\bar{\beta}_0$ with different $\bar{\beta}_s$ and $\bar{\beta}_p$, which is account for the reason why $\Delta\sigma_{pu}^{c}$ and $\Delta\sigma_{pu}^{t}$ scatter so much.

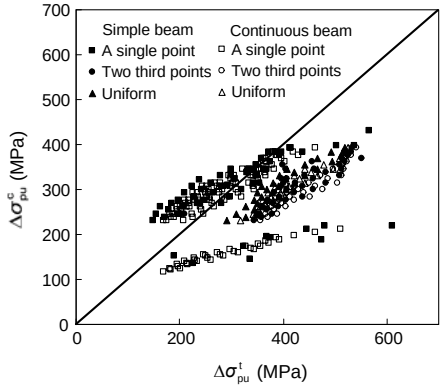

Fig. 11 Comparison between $\Delta\sigma_{pu}^{t}$ and $\Delta\sigma_{pu}^{c}$ from Eq. (23)

7. Chinese regulations JGJ 92-2004 for unbonded prestressed concrete technology

$$\sigma_{pu}=\sigma_{pe}+\Delta\sigma_p, \tag{24}$$

$$\Delta\sigma_p=(240-335\beta_0)(0.45+5.5h/L), \tag{25}$$

$$\sigma_{pe}\le\sigma_{pu}\le f_{pu},\ \beta_0\le 0.4.$$

It leads to the predicted $\Delta\sigma_{pu}^t$ to multiply the design values of the ultimate stress in the tendons predicted from Eq. (25) by subentry coefficient γ_s (=1.2) of the material strength and to subtract the effective prestress σ_{pe}. The comparison of $\Delta\sigma_{pu}^c$ with $\Delta\sigma_{pu}^t$ is shown in Fig. 12, where the data plots are mostly under the correlation line. The reason is similar to the discussions for Eq. (25). Note that f_y is the yield stress of the non-prestressing steel and f_{cm} is conceret compressive strength when calculation of β_0.

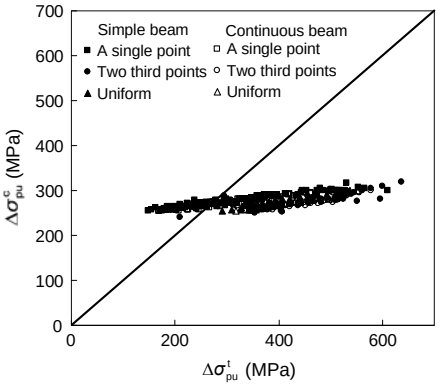

Fig. 12 Comparison between $\Delta\sigma_{pu}^t$ and $\Delta\sigma_{pu}^c$ from Eq. (25)

8. Jin *et al.* (2003) equation

$$\sigma_{pu}=\sigma_{pe}+\frac{(500-770\bar{\beta}_0)(0.4+6/(L/d_p))}{1.5}. \tag{26}$$

Multiplying the design values of the ultimate stress in the tendons predicted from Eq. (26) by 1.2 and subtracting σ_{pe} result in the predicted $\Delta\sigma_{pu}^c$. The comparison of $\Delta\sigma_{pu}^c$ with $\Delta\sigma_{pu}^t$ is shown in Fig. 13, where the data plots are mostly under the correlation line, which shows that Eq. (26) predicts conservative values. As shown in Fig. 13, $\Delta\sigma_{pu}^c$ and $\Delta\sigma_{pu}^t$ scatter so much because Eq. (26) does not take account of the effect of the distribution of the unbonded tendons, loading type, numbers of spans and the same $\bar{\beta}_0$ with different $\bar{\beta}_s$ and $\bar{\beta}_p$. Note that $\bar{\beta}_0=(\sigma_{pe}A_p+f_yA_s)/(f_{cm}bh_p)$, where f_y is the yield stress of the non-prestressing steel and f_{cm} is conceret compressive strength.

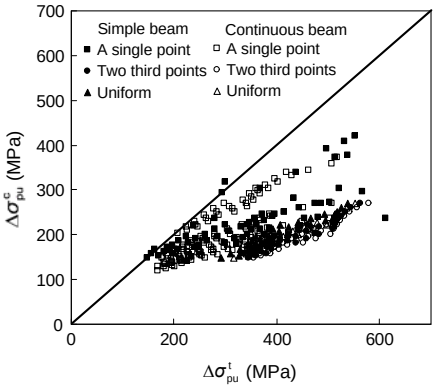

Fig. 13 Comparison between $\Delta\sigma_{pu}^t$ and $\Delta\sigma_{pu}^c$ from Eq. (26)

9. Harajli Eq. (I) (1990)

$$\sigma_{pu}=\sigma_{pe}+70+\frac{f_c'}{100\rho_p}\left(0.4+\frac{8}{L/d_p}\right) \le \sigma_{pe}+414 \text{ and } f_{py}. \tag{27}$$

Substituting the test values of the material strength of test beams into Eq. (27) and then $\Delta\sigma_{pu}^c$ is predicted. The comparison of $\Delta\sigma_{pu}^c$ with $\Delta\sigma_{pu}^t$ is shown in Fig. 14, where no data plots are over the correlation line, which shows that Eq. (27) predicts conservative values. This is due to Eq. (27) not taking the effect of the non-prestressing reinforcements, loading type, number of spans and distribution of unbonded tendons into account.

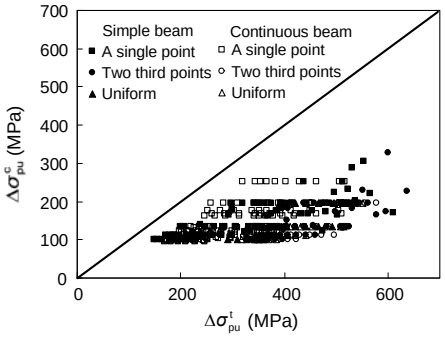

Fig. 14 Comparison between $\Delta\sigma_{pu}^t$ and $\Delta\sigma_{pu}^c$ from Eq. (27)

10. Harajli Eq. (II) (1990)

$$\Delta\sigma_{\mathrm{p}} = \gamma(\alpha - \beta c / h_{\mathrm{p}}) f_{\mathrm{ptu}}, \tag{28}$$

$$c = \frac{A_{\mathrm{p}}(\sigma_{\mathrm{pe}} + \alpha\gamma f_{\mathrm{ptk}}) + A_{\mathrm{s}} f_{\mathrm{y}} - A_{\mathrm{s}}' f_{\mathrm{y}} - c_{\mathrm{f}}}{0.85\beta_1 f_{\mathrm{c}}' b_{\mathrm{w}} + \beta\gamma A_{\mathrm{p}} f_{\mathrm{ptk}} / h_{\mathrm{p}}},$$

$$c_{\mathrm{f}} = 0.85 f_{\mathrm{c}}'(b - b_{\mathrm{w}}) h_{\mathrm{f}},$$

$$\gamma = \left[1.0 + \frac{1.0}{(L / h_{\mathrm{p}})(0.95 / f + 0.05)}\right](n_0 / n),$$

where c is the neutral axis depth in the critical section at ultimate state, n/n_0 is the ratio of number of loaded spans to total number of spans in the member, f is the load geometry factor: f=3 for two equal third point loads; f=6 for uniform loads, and f=∞ for a concentrated load. α and β are parameters whose magnitudes depend on the spread of plasticity in the member at an ultimate flexural strength state and are related in effect to the geometry of applied loads: α=0.4, β=0.70 when f=3; α=2.5, β=0.44 when f=6; and α=0.1, β=0.18 when f=∞.

Substituting the tested values of material strength of test beams into Eq. (28), results in the predicted $\Delta\sigma_{\mathrm{pu}}^{\mathrm{c}}$. The comparison of $\Delta\sigma_{\mathrm{pu}}^{\mathrm{c}}$ with $\Delta\sigma_{\mathrm{pu}}^{\mathrm{t}}$ is shown in Fig. 15, where the values of $\Delta\sigma_{\mathrm{pu}}^{\mathrm{c}}$ are obviously higher than $\Delta\sigma_{\mathrm{pu}}^{\mathrm{t}}$ for beams under two third point loads, and as a whole, the deviation between $\Delta\sigma_{\mathrm{pu}}^{\mathrm{c}}$ and $\Delta\sigma_{\mathrm{pu}}^{\mathrm{t}}$ is great. The reason is because the stress increase in unbonded tendons at an ultimate state is over-predicted for beams under two third point loads but under-predicted for beams under uniform loads though the effect of loading type is considered in Eq. (28).

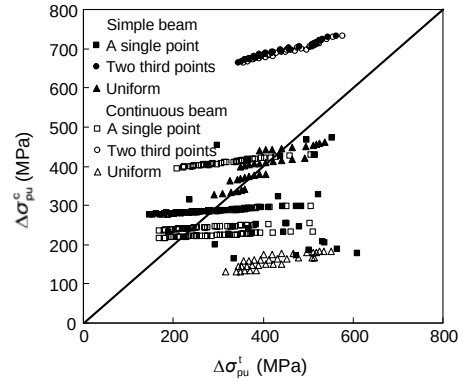

Fig. 15 Comparison between $\Delta\sigma_{\mathrm{pu}}^{\mathrm{t}}$ and $\Delta\sigma_{\mathrm{pu}}^{\mathrm{c}}$ from Eq. (28)

11. Du and Tao (1985) equation

$$\sigma_{\mathrm{pu}} = \sigma_{\mathrm{pe}} + 786 - 1920 q_0, \tag{29}$$

$$q_0 = (f_{\mathrm{y}} A_{\mathrm{s}} + \sigma_{\mathrm{pe}} A_{\mathrm{p}}) / (f_{\mathrm{c}}' b h_{\mathrm{p}}) \le 0.38.$$

Adopting the average values of material strength of test beams to Eq. (29), $\Delta\sigma_{\mathrm{pu}}^{\mathrm{c}}$ is predicted. The comparison of $\Delta\sigma_{\mathrm{pu}}^{\mathrm{c}}$ with $\Delta\sigma_{\mathrm{pu}}^{\mathrm{t}}$ is shown in Fig. 16, where the values of $\Delta\sigma_{\mathrm{pu}}^{\mathrm{c}}$ are higher than $\Delta\sigma_{\mathrm{pu}}^{\mathrm{t}}$ in beams under a concentrated mid-span load, but the reverse happens in the beams under two third point or uniform loads. The reason is because of Eq. (29) derived from the testing data in simple beams under two third point loads. The beams under a concentrated mid-span load suffer relatively small deformation at an ultimate state, so the ultimate stress increase in unbonded tendons is smaller.

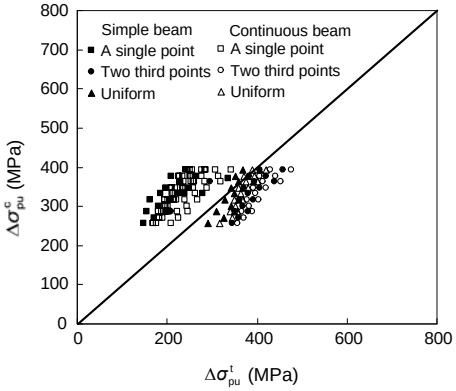

Fig. 16 Comparison between $\Delta\sigma_{\mathrm{pu}}^{\mathrm{t}}$ and $\Delta\sigma_{\mathrm{pu}}^{\mathrm{c}}$ from Eq. (29)

12. Xu *et al*. (1995) equation

$$\Delta\sigma_{\mathrm{pu}} = (500 - 770\bar{\beta}_0) k_l k_h \Omega, \tag{30}$$

where k_l is the continuous span reduction coefficient, $k_l = \dfrac{l}{\eta_{\mathrm{u}} \sum l}$, k_h is the span-depth ratio modifier coefficient, $k_h = 0.7 + 10/(l/h)$, ΣL is the total span length between end anchorages, η_{u} is the unbonded tendon effective transfer coefficient, η_{u}=0.7–1.0, Ω is the reduction coefficient representing the effect of

curve shape and position of unbonded tendons, Ω=1 for one span beams with straight tendons; Ω≈2/3 for one span beams with parabola tendons; Ω≈1/2 for multi-spans beams with parabola tendons.

Adopting the average values of material strength of test beams to Eq. (30) yields the predicted $\Delta\sigma_{pu}^{c}$. The comparison of $\Delta\sigma_{pu}^{c}$ with $\Delta\sigma_{pu}^{t}$ is shown in Fig. 17. $\Delta\sigma_{pu}^{c}$ predicted by Eq. (30) is larger than $\Delta\sigma_{pu}^{t}$ for simple beams under concentrated load, and agrees with $\Delta\sigma_{pu}^{t}$ for beams under two third point loads, but is conservative in comparison with $\Delta\sigma_{pu}^{t}$ for continuous beams.

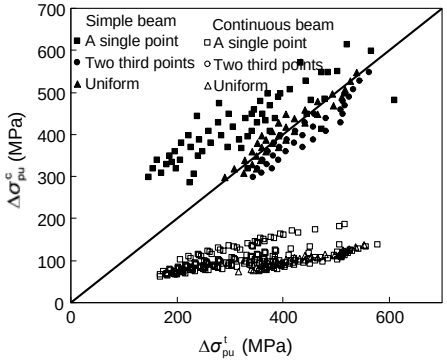

Fig. 17 Comparison betwe $\Delta\sigma_{pu}^{t}$ and $\Delta\sigma_{pu}^{c}$ from Eq. (30)

13. Chen and Zhao (1993) equation

$$\sigma_{pu}=\sigma_{pe}+618.3(1-2.094\bar{\beta}_0). \tag{31}$$

The predicted $\Delta\sigma_{pu}^{c}$ is found by substituting material strength of test beams into Eq. (31). The comparison of $\Delta\sigma_{pu}^{c}$ with $\Delta\sigma_{pu}^{t}$ is shown in Fig. 18. $\Delta\sigma_{pu}^{c}$ agrees with $\Delta\sigma_{pu}^{t}$ for beams under concentrated load, but is lower than $\Delta\sigma_{pu}^{t}$ for beams under other types of loading. This is due to the fact that the equation is derived from the test results for beams under a single concentrated load. Furthermore, Eq. (31) only accounts for the effect of combined reinforcement index, but ignores the influence of the prestressing reinforcement index, non-prestressed reinforcement index, and the span-depth ratio.

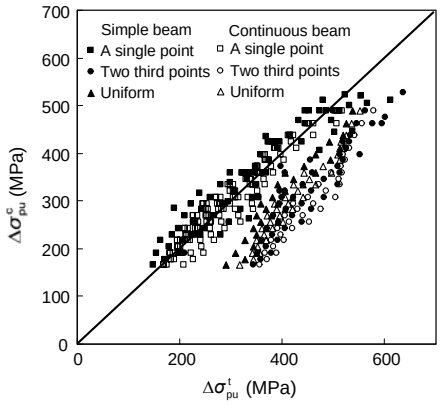

Fig. 18 Comparison between $\Delta\sigma_{pu}^{t}$ and $\Delta\sigma_{pu}^{c}$ from Eq. (31)

14. Naaman and Alkhairi (1991) equation

$$\sigma_{pu}=\sigma_{pe}+\Omega_u E_p \varepsilon_{cu}\left(\frac{d_p}{c}-1\right)\frac{L_1}{L_2}\le 0.94 f_{py}, \tag{32}$$

where $\Omega_u=1.5/(L/d_{ps})$ for beams under a concentrated load; $\Omega_u=3.0/(L/d_{ps})$ for beams subjected to third point or uniform loads. E_p is the elastic modulus of prestressed steel, ε_{cu} is the ultimate compression strain of concrete, set ε_{cu}=0.003, L_1 is the length of loaded span or sum of lengths of loaded spans influenced by the same tendon, and L_2 is the length of tendon between end anchorages.

Adopting the tested values of the material strength in tested beams to Eq. (32) leads to the predicted $\Delta\sigma_{pu}^{c}$. The comparison of $\Delta\sigma_{pu}^{c}$ with $\Delta\sigma_{pu}^{t}$ is shown in Fig. 19, where all the data plots are under the correlation line; thus, Eq. (32) predicts conservative values.

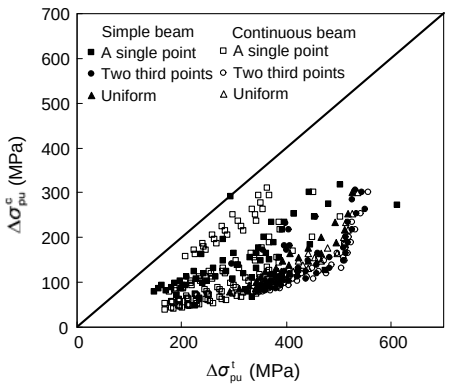

Fig. 19 Comparison between $\Delta\sigma_{pu}^{t}$ and $\Delta\sigma_{pu}^{c}$ from Eq. (32)

15. Equation proposed in this study

For simple beams:

$$\Delta\sigma_{\mathrm{pu}}=\begin{cases}663-1137\beta_{\mathrm{p}}-703\beta_{\mathrm{s}}, \text{ third point,}\\ (560-1449\beta_{\mathrm{p}}-837\beta_{\mathrm{s}})(0.86+2.4h/L), \\ \qquad\qquad \text{single point,}\\ 631-1144\beta_{\mathrm{p}}-735\beta_{\mathrm{s}}, \text{ uniform.}\end{cases} \tag{33}$$

For continuous beams:

$$\Delta\sigma_{\mathrm{pu}}=\begin{cases}677-1075\beta_{\mathrm{p}}-741\beta_{\mathrm{s}}, \text{ third point,}\\ (632-1408\beta_{\mathrm{p}}-834\beta_{\mathrm{s}})(0.8+2h/L), \\ \qquad\qquad \text{single point,}\\ 659-1128\beta_{\mathrm{p}}-833\beta_{\mathrm{s}}, \text{ uniform.}\end{cases} \tag{34}$$

Substituting the tested values of the material strength in the tested beams into Eqs. (33) and (34) yields the predicted $\Delta\sigma_{\mathrm{pu}}^{\mathrm{c}}$. The comparison of $\Delta\sigma_{\mathrm{pu}}^{\mathrm{c}}$ with $\Delta\sigma_{\mathrm{pu}}^{\mathrm{t}}$ is shown in Fig. 20, where $\Delta\sigma_{\mathrm{pu}}^{\mathrm{c}}$ predicted by Eqs. (33) and (34) agrees well with $\Delta\sigma_{\mathrm{pu}}^{\mathrm{t}}$, which shows that the prediction equations of the ultimate stress increase in unbonded tendons proposed in this study have adequate precision.

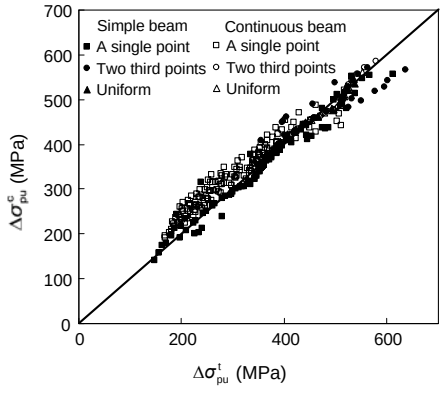

Fig. 20 Comparison between $\Delta\sigma_{\mathrm{pu}}^{\mathrm{t}}$ and $\Delta\sigma_{\mathrm{pu}}^{\mathrm{c}}$ from Eq. (33) and Eq. (34)

3 Conclusions

1. Based on the results of model test and simulation analysis, prediction equations for design values of stress and stress increase in unbonded tendons in beams at an ultimate state are developed, considering rationally the influence of loading types, non-prestressed reinforcement index β_{s}, prestressing reinforcement index β_{p}, and span-depth ratio L/h.

2. Prediction equations of tendon at ultimate as proposed by this study and other researches, are analyzed and compared for verification.

The ultimate stress increase in unbonded tendons in frame beams and continuous beams of more than 3 spans should be considered for the further study.

References

A23.3-94. Design of Concrete Structures. Canadian Standards Association. Rexdale, Ontario, Canada.

ACI318-02. Building Code Requirements for Structural Concrete (ACI 318-02) and Commentary (ACI 318R-02). American Concrete Institute, Michigan.

Ariyawardena, N.D., 2002. Design of precast prestressed concrete members using external prestressing. *PCI Journal*, **47**(2):84-91.

Barakat, S., Bani-Hani, K., 2004. Multi-objective reliability-based optimization of prestressed concrete beams. *Structural Safety*, **26**(3):311-342. [doi:10.1016/j.strusafe.2003.09.001]

BS8110-1-1997. Structural Use of Concrete, Part 1—Code of Practice for Design and Construction. British Standards Institution, London.

Chen, X.B., Zhao, G.F., 1993. Investigation and reliability analysis of ultimate strength of unbonded partially prestressed concrete beams. *Journal of Dalian University of Technology*, **33**(5):548-551 (in Chinese).

Du, G.C., Tao, X.K., 1985. A study of the ultimate stress of unbonded tendons in partially prestressed concrete beams. *Journal of Building Structures*, **6**(6):2-13 (in Chinese).

Harajli, M.H., 1990. Effect of span-depth ratio on the ultimate steel stress in unbonded prestressed concrete member. *ACI Structural Journal*, **87**(8):305-312.

JGJ 92-2004. Technical Specification for Concrete Structures Prestressed with Unbonded Tendons. China Academy of Building Research, Beijing.

Jin, W.L., Zhao, Y.X., Lü, Z.T., 2000. Ultimate stress of unbounded prestressed tendons. *Journal of Zhejiang University (Engineering Science)*, **34**(4):393-397 (in Chinese).

Liu, F., Chen, X.B., 2003. Experimental study of unbonded prestressed concrete beams under concentrated load. *Journal of Hefei University of Technology*, **24**(5): 880-884 (in Chinese).

Naaman, A.E., Alkhairi, F.M., 1991. Stress at ultimate in unbonded prestressing tendons: part 1—evaluation of the state-of-art. *ACI Structural Journal*, **88**(5):683-692.

Tao, X.K., 1993. Unbonded Prestressed Concrete Structure Design and Construction. Earthquake Publishing Company, Beijing, China, p.20-50 (in Chinese).

Tao, X.K., Wang, Y., Du, G.C., 1989. Deflection estimation for unbonded partially prestressed concrete flexural members. *Journal of Building Structures*, **10**(1):20-27 (in Chinese).

Wang, X.D., 2005. Research on Law of Stress Increase in Concrete Flexural Members. MS Thesis, Harbin Institute of Technology, Harbin, China (in Chinese).

Xu, J.S., Lin, C.Z., Hong, W.E., 1995. Study on structural behavior of waffle slab floor with unbonded prestressed tendons and non-prestressed steel. *Journal of Building Structures*, **16**(1):3-14 (in Chinese).

Zheng, W.Z., Zheng, X., Wang, Y., 2005. Calculation of ultimate stress of unbonded tendons in continuous prestressed concrete beam. *Building Structure*, **35**(7): 67-71 (in Chinese).

Zhou, W., 2005. Research on Three Fundamental Issues in Design of Prestressed Concrete Structures. PhD Thesis, Harbin Institute of Technology, Harbin, China (in Chinese).